JOURNAL OF SOLID STATE CHEMISTRY 66, 204–224 (1987)

Electrochemical, Structural, and Physical Properties of the Sodium Chevrel Phases $Na_xMo_6X_{8-y}I_y$ (X = S, Se and y = 0 to 2)

J. M. TARASCON AND G. W. HULL

Bell Communication Research, Murray Hill, New Jersey 07974

AND P. MARSH AND TER HAAR

AT&T Bell Laboratories, Murray Hill, New Jersey 07974

Received February 24, 1986; in revised form April 28, 1986

We report the synthesis and structural and physical properties of the sodium Chevrel phases $Na_xMo_6X_{8-y}I_y$ (X = S, Se; $0 \leq y \leq 2$). These materials were synthesized by means of electrochemical reactions using $Na/Mo_6X_{8-y}I_y$ test cells. Structural changes induced by sodium intercalation were studied by *in situ* X-ray diffraction measurements. Cycling data indicates that the sodium intercalation process into $Mo_6X_{8-y}I_y$ is initially irreversible and results in compounds of formula $Na_xMo_6X_{8-y}I_y$ with x_{min} decreasing from 1 to 0 as y increases from 0 to 2. However, after the first cycle the cells are *readily reversible* over several cycles. The analysis of the discharge curves show that the maximum sodium content (x_{max}) into the $Mo_6X_{8-y}I_y$ matrix decreases from 4 to 2 with y rising from 0 to 2. This behavior is consistent with the electronic structure of the "host" established from band structure calculations. The anomalies observed in the electrochemical curves ($V(x)$ and dx/dV vs V) correlated perfectly with the observed structural changes. Structural studies for the $Na_xMo_6X_8$ system revealed the presence of three single-phase compounds, $R_1(x \simeq 1)$, $T_1(x \simeq 3)$, and $T_2(x \simeq 4)$ where R and T correspond to rhombohedral and triclinic unit cells, respectively, the triclinic phases being extremely moisture sensitive. The range of existence of these phases turns out to be strongly dependent upon iodine substitution. Magnetic susceptibility measurements of the $Na_3Mo_6X_8$ phase suggested a structural instability at 40 and 70 K for the sulfide and selenide, respectively, but neither superconducts down to 1.5 K. Conversely, both $Na_1Mo_6X_8$ phases, which do not exhibit low-temperature anomalies in the temperature dependence of the susceptibility, become superconducting at 9 K.

Introduction

The Chevrel phase compounds of formula $M_xMo_6X_8$ (X = chalcogens) have been intensively studied mainly because of their fascinating superconducting (high critical temperatures, T_c, and critical magnetic fields) and superionic properties (*1, 2, 3*). These properties have been found to strongly depend upon both the nature of the ternary element (M) and its content (x) as well as upon the nature of the anion (X).

Most of these phases adopt an hexagonal–rhombohedral structure (*4, 5*). The building blocks are Mo_6X_8 clusters consisting of a molybdenum octahedron surrounded by eight chalcogen atoms forming the corners of a cube. The three-dimensional packing of Mo_6S_8 clusters leaves empty cavities which can accommodate the ternary metal atoms. Large atoms (such as Pb^{2+}, Sn^{2+}, etc.) sit on the cluster cube diagonal ($\bar{3}$ axis) while small atoms (such as Cu^+, Li^+, etc.) sit on concentric rings of tet-

0022-4596/87 $3.00

rahedral sites centered about the $\bar{3}$ axis, resulting in what are refered to as type I and type II Chevrel phases, respectively (*2*). Type I phases possess a rhombohedral angle (α_r) lower than 90° and exist for a defined value of x ($x \simeq 1$), whereas type II exhibit an α_r higher than 90° and exist over a wide range of composition for the ternary element cation (for example, $2 < x < 4$ for the $Cu_xMo_6S_8$ system). Although Na^+ has the same ionic radius as Cu^+, previous work (*6*) seemed to indicate that $NaMo_6S_8$ is a type I phase.

In addition to superconductivity, Dudley *et al.* (*7, 8*) have shown that type II compounds also exhibit a high ionic conductivity. The high mobility of the guest atoms (M) in these open framework type structures led to the synthesis of new metastable binary or ternary Chevrel phases by means of low-temperature chemical and electrochemical reactions. The lithium and copper systems were the subject of a large amount of theoretical and experimental work (*8–14*) mainly because of the possible use of Mo_6X_8 or $Cu_2Mo_6X_8$ as cathode materials in room temperature secondary lithium batteries. For instance it has been observed (*11*) that Mo_6X_8 can reversibly accommodate up to four lithium atoms per formula unit leading to a theoretical density of 240 Whr/kg.

In contrast to lithium, the sodium system ($Na_xMo_6S_8$) has been poorly studied and the few results reported in the literature are quite contradictory. For instance, Chevrel (*15*) reported a compound of formula $Na_2Mo_2S_3$ and Alekscevskii (*16*) found a single-phase product at $x = 2$, whereas an air stable single-phase compound at $x = 1$ has been recently reported by Potel (*6*). Schollhorn *et al.* (*17, 18*) have studied the electrochemical intercalation of several atoms into the binary phases Mo_6X_8, including sodium. The authors did not find any evidence for single phases at $x = 1$ or 2 but did find a phase at $x \simeq 3.6$. Furthermore, they mentioned that the ternary phase $Na_xMo_6S_8$, like $Li_xMo_6S_8$, is moisture sensitive and rapidly converts to Mo_6S_8 when exposed to water suggesting a high mobility of sodium atoms into the Mo_6S_8 matrix. To our knowledge no work has been reported for the homolog selenide system $Na_xMo_6Se_8$.

In order to find a clue to the above puzzles we started on a complete study of the sodium Chevrel phases. In this paper we first report the electrochemical insertion of sodium into the binary phases, Mo_6X_8, as well as the room temperature phase diagram of both $Na_xMo_6X_8$ (X = S, Se) systems established by means of *in situ* X-ray diffraction measurements. We found that sodium intercalation is irreversible resulting in the air stable $Na_1Mo_6S_8(Se_8)$ phases. We then extended this study to the binary molybdenum halochalcogenide phases of formula $Mo_6X_{8-y}I_y$ and we found that increasing iodine substitution enhances the reversibility of the sodium intercalation process. In addition we present the measurements of the superconducting critical temperatures as well as magnetic susceptibilities as a function of temperature for each single-phase product. Finally, we discuss these data in relation to those previously obtained on similar compounds having lithium instead of sodium as guest atoms.

Experimental

The binary molybdenum chalcogenides Mo_6X_8 were synthesized at low temperatures (60°C) by oxidation of $Cu_2Mo_6X_8$ with a solution of iodine in acetonitrile as described earlier (*19*). In contrast the halochalcogenides $Mo_6X_{8-y}I_y$ (y = 0.5, 1, 2 when X = selenium and $y = 2$ when X = sulfur, respectively) were directly prepared by reaction of appropriate amounts of H_2 reduced molybdenum powder (99.99%), sulfur or selenium (99.999%), and freshly

sublimed iodine at high temperatures (1000–1100°C) in evacuated silica tubes for several days (*17*). After such a treatment the resulting materials were washed with acetonitrile to remove traces of unreacted iodine and then X-rayed. The compounds were single phase and the lattice parameters deduced from a least-square fitting of the low-angle peaks ($10° < 2\theta < 60°$) are similar to the already published values (*29*).

Swagelock test cells were used for the electrochemical insertion of sodium into the $Mo_6X_{8-y}I_y$ phases. The cells were prepared in a helium atmosphere with $Mo_6X_{8-y}I_y$ as cathode and a half-inch diameter stainless steel disk pasted with sodium metal as anode. Both electrodes were separated by porous glass paper soaked in 1 *M* $NaClO_4$ in propylene carbonate as electrolyte. The assembled cells were automatically tested as described earlier (*20*). The cell voltage $V(x)$ was measured as a function of time while the cell charged or discharged at constant current rate. Changes in x in $Na_xMo_6X_{8-y}I_y$ are proportional to changes in time and could be calculated from both the current used and the amount of cathode material. The differential capacity curves (dx/dV vs v or dV/dx vs x) reported in this paper are directly derived from $V(x)$.

Structural changes of the host materials with respect to sodium intercalation were studied by means of *in situ* X-ray diffraction measurements using a specially designed electrochemical cell (Fig. 1) mounted on a Rigaku Miniflex diffractometer. The cathode material is mixed with 1,2-propanediol and then evaporated at 200°C in flowing argon onto a beryllium disk. The disk is then glued into the cylindrical recess on the back of the top cell window. The beryllium disk allows the X-rays to reach the sample and further serves as a standard to align the cell. The stainless steel top with the electrode is then transferred to a dry box where the cell is constructed (Fig. 1). The sodium metal is then pasted or melted onto the reservoir machined into the cell base, two pieces of glass paper are then placed on top of the shiny sodium metal surface, and enough electrolyte added to wet the separator. The cell top and base were then put together with a Teflon gasket as a separator. To ensure physical contact among the cell components, the cell top and base were squeezed by means of four nylon screws. The purpose of the Teflon gasket is twofold; first, to prevent electrical contact between the two electrodes and second, to have an airtight seal. The assembled cell

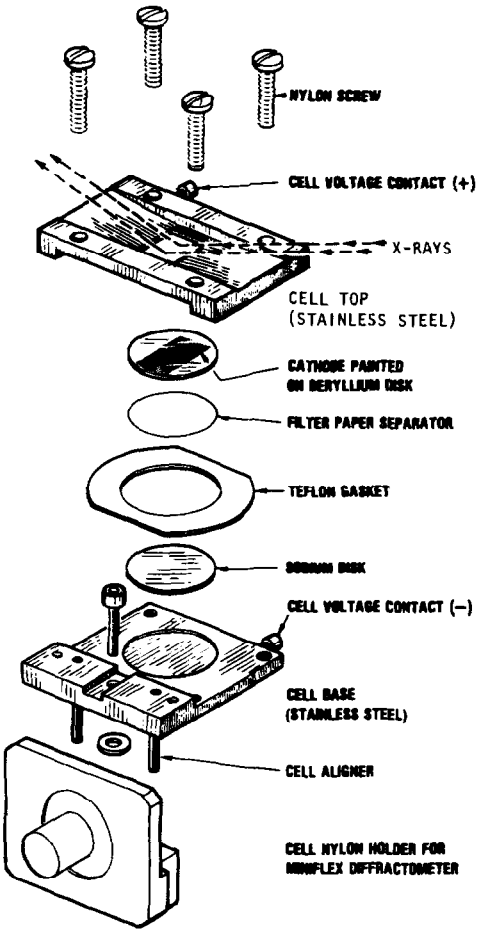

FIG. 1. Design of the electrochemical cell used for *in situ* X-Ray diffraction studies of the sodium intercalation compounds $Na_xMo_6X_{8-y}I_y$.

was placed on a nylon holder, removed from the dry box, and then mounted on the diffractometer. The cell alignment is done by means of a set screw which moves the cell chamber back and forth along the alignment pins. Finally, cathode and anode were electrically connected through a scanning potantiostat (Model 362) for testing. In such measurements X-ray powder diffraction patterns are collected at different values of x, between $10° < 2\theta < 60°$, while the cell is charged and discharged at constant current. In order to be close to equilibrium conditions, current rates as low as 15 $\mu A/cm^2$ were used.

Large amounts of material (200 mg) for physical studies and chemical analysis were also made electrochemically using swagelock test cells. In such cases the cells were discharged and/or recharged at very low current and were maintained at the potential chosen, corresponding to a special value of x, for several days in order to equilibrate. The resulting sodium phases were X-rayed without being exposed to air by means of an airtight X-ray holder. The X-ray diffraction patterns gave sharp peaks, strongly suggesting that equilibrium conditions had been reached. The sodium content (x) in these materials was determined by atomic absorption analysis with an accuracy of about ±3%.

The magnetic susceptibility (χ_g) and the superconducting transition temperature of these materials were determined using a SHE (Model 905) variable temperature susceptometer with a 5 tesla superconducting magnet. The apparatus is a SQUID based flux measuring system connected to two pairs of counterwound coil pairs. In the peak-to-peak mode the sample is cycled through both coils resulting in a peak-to-peak signal directly proportional to the total magnetic moment (M) of the sample. To obtain the superconducting critical temperature T_c, the system is operated in a continuous mode whereby the sample is held constant in one of the coil pairs and the flux change is monitored while varying the temperature. The T_c values were defined as the onset of the superconducting transition. A Teflon holder with an airtight fitting top was used for both magnetic and superconducting measurements of air sensitive compounds.

Results

Electrochemical Data

It is important to recall that the voltage of a $Na/NaMo_6X_8$ electrochemical cell is directly proportional to the sodium chemical potential in $Na_xMo_6X_8$ (taking Na/Na^+ as reference zero) for the reaction

$$x\text{Na} + \text{Mo}_6X_8 \rightarrow \text{Na}_x\text{Mo}_6X_8.$$

Thus the cell voltage will give us direct thermodynamic data from which interesting structural and electronic information can be deduced. For instance, when considering the system as a pseudo-binary, plateaus in the voltage composition curves $V(x)$ are characteristic of two-phase regions whereas ranges of nonzero slope are reminiscent of single-phase regions (*21*). However, difficulty arises in predicting phase mixtures occurring over a small coexistence range from the $V(x)$ curves. The differential capacity curves are of great help in solving this problem since multiphase domains appear as peaks in the dx/dV vs V plots. Recent work (*22, 23*) even showed that the shape of these peaks (asymmetric or symmetric) can allow us to determine whether the transition is of first or second order, respectively. Therefore, as both second order phase transitions and solid solutions give rise to symmetric peaks in dx/dV vs V plots, only *in situ* X-ray diffraction measurements can distinguish between these two possibilities.

We now present the electrochemical and structural results for the $Na_xMo_6S_8$, $Na_xMo_6Se_{8-y}I_y$ (y = 0, 0.5, 1, 2), and

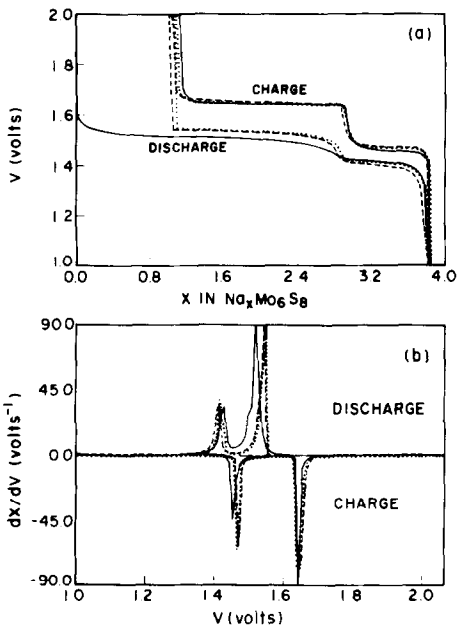

FIG. 2. Typical behavior of a $Na/Na_xMo_6S_8$ cell operating at a current density of 100 $\mu A/cm^2$ over several cycles. Solid, dotted, and dashed line represent the first, second, and third cycle, respectively. (a) Voltage plotted as a function of x. (b) dx/dV plotted as a function of V.

$Na_xAgMo_6S_8$ systems separately with regard to the above remarks. The electrochemical behavior over several cycles of a cell based on Mo_6S_8 as cathode material is reported in Fig. 2. Several interesting features can be observed. Mo_6S_8 can take up four sodium atoms on discharge down to 1 V but only three of them can be removed on recharge up 2.7 V. Attempts to completely recharge the cell with voltage as high as 3.2 V have been unsuccessful. A loss in capacity in the first cycle is generally observed for secondary alkali metal batteries and is mainly due to the presence of cathode particles which become electrically disconnected on recharge. However this loss never exceeds 10%. The 25% loss presently observed on the first cycle suggests an irreversible sodium intercalation process. After the first cycle the Na/Mo_6S_8 cell is readily reversible between $x = 1$ and $x = 4$ and retains its capacity over several cycles.

The voltage composition curves show several anomalies most likely correlated to single-phase products near the nominal compositions $x = 0$, 3, and 3.9 on discharge and $x = 3.9$, 3, and 1 on recharge. These phases are connected by plateaus which appear as peaks in the differential capacity curves dx/dV vs V (Fig. 2b). The voltage at which these two peaks occur shifts between the first and second discharge and finally stabilizes at 1.44 and 1.54 V on subsequent discharges. Both peaks are asymmetric suggesting two first order phase transitions.

To substantiate the above suggestions *in situ* X-ray diffraction measurements were performed. On a single cycle more than 40 X-ray powder diffraction patterns have been taken in order to detect subtle sodium-induced lattice instabilities. Figure 3 shows some of these X-ray patterns (denoted as a, b, c, . . .) which have been taken at positions labeled a, b, c, . . . on the electrochemical curve. At $x = 0$ (pattern a) we have the rhombohedral phase R_0. As the sodium intercalation proceeds, the lines of the R_0 phase do not shift, but several extra lines due to a second phase begin to appear (pattern b). This second phase becomes predominant as x increases and unique at $x = 3$ (pattern c). All the peaks of this new single phase were completely indexed as a triclinic cell (denoted as T_1) whose lattice parameters are reported in Table I. The quality of this fit is shown in Table II. Further intercalation results in the onset of a third phase which becomes unique at $x = 3.9$. The diffraction patterns of this new phase were fitted successfully using another triclinic unit cell (denoted as T_2). The lattice parameters are reported in Table I. One can note that the $T_1 \leftrightarrow T_2$ transition results in a dramatic increase of the lattice dimensions a, b, and c of about 0.2, 0.1, and 0.2 Å, respectively. However, one of

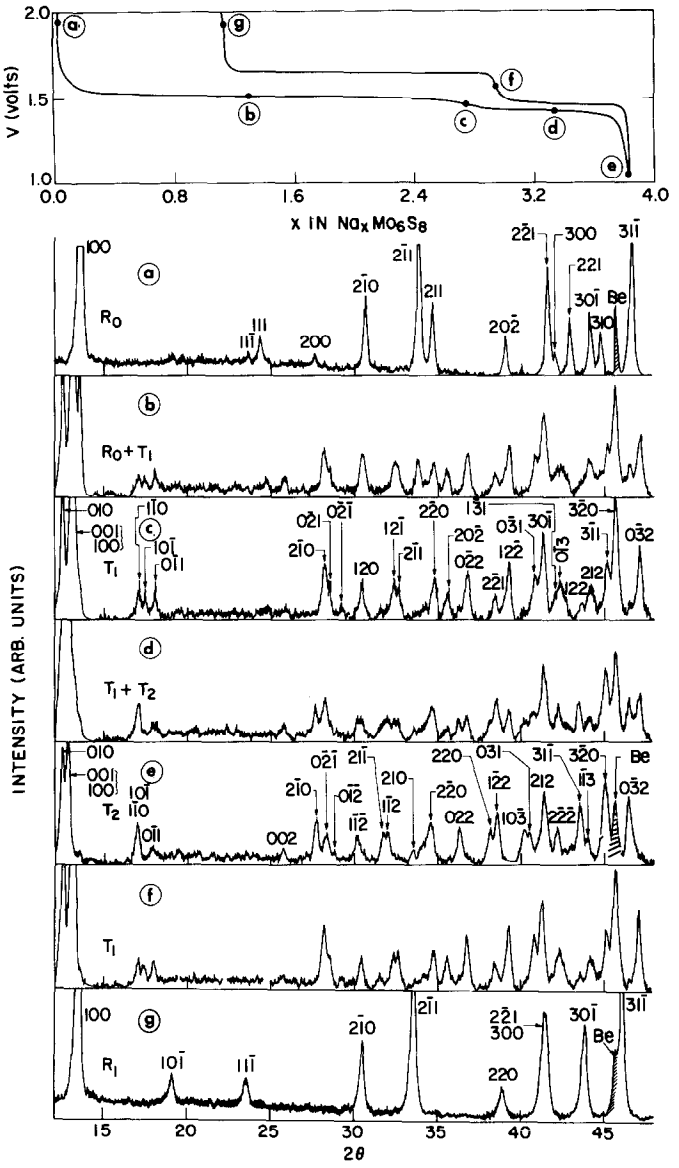

FIG. 3. X-ray diffraction patterns of the $Na_xMo_6S_8$ phases collected while a $Na/Na_xMo_6S_8$ cell was cycled at a current density of 20 $\mu A/cm^2$, at positions labeled a, b, c, d, e, f, and g on the $V(x)$ curve (top plot). Diffraction planes are shown above each peak.

the most remarkable results is the large unit cell volume increase (of about 30%) induced by intercalation of four sodium atoms into the Mo_6X_8 matrix. The presence of two sets of lines on the X-ray diffraction patterns b and d unambiguously indicates that both $R_0 \rightarrow T_1$ and $T_1 \leftrightarrow T_2$ transitions are of first order as already suggested from the dx/dV vs V plots.

We should state that in general, triclinic

TABLE I

CRYSTALLOGRAPHIC PARAMETERS AND SUPERCONDUCTING TRANSITION TEMPERATURES T_c AS A FUNCTION OF COMPOSITION IN THE SERIES $Na_xMo_6X_{8-y}I_y$ (X = S, Se; y = 0, 0.5, 1, 2)

Compounds	x Atomic absorption analysis	x Electro-chemical data	Iodine content atomic absorption analysis	a_h (Å)	c_h (Å)	V_h (Å^3)	a_r (Å)	α_r (°)		V_r (Å^3)	T_c (K)
Mo_6S_8 (R_0)	—	—	—	9.201(0)	10.880(8)	797	6.43	91.6		265.6	1.6
$Na_xMo_6S_8$ (R_1)	0.98	1.03	—	9.230(0)	11.328(7)	835.9	6.531	89.92		278.6	9
$Na_xMo_6S_8$ (T_1)	3.04	3.1	—	a = 6.706(3)	b = 6.991(4)	c = 6.695(3)	α = 90.48(5)	β = 97.30(5)	γ = 97.33(5)	308.9	<1
$Na_xMo_6S_8$ (T_2)	3.85	3.90	—	a = 6.925(3)	b = 7.100(4)	c = 6.932(4)	α = 89.68(4)	β = 94.90(5)	γ = 95.46(5)	338.1	<1
$Mo_6S_6I_2$	—	—	2.01	9.649(0)	10.453(6)	842.9	6.57	94.48		280.9	13.2
Mo_6Se_8 (R_0')	—	—	—	9.570(1)	11.152(4)	884	6.66	91.85		294.6	6.2
$Na_xMo_6Se_8$ (R_1')	0.97	1.05	—	9.590(2)	11.758(5)	936	6.78	89.86		312.0	8.9
$Na_xMo_6Se_8$ (T_1')	2.95	3.05	—	a = 6.979(3)	b = 7.136(3)	c = 6.830(3)	α = 91.22(4)	β = 97.17(5)	γ = 97.04(4)	334.7	<1
$Na_xMo_6Se_8$ (T_2')	3.9	3.95	—	a = 7.167(2)	b = 7.306(2)	c = 7.110(4)	α = 90.14(4)	β = 97.83(4)	γ = 96.47(3)	366.5	<1
$Mo_6Se_{7.5}I_{0.5}$ (R_0'')	—	—	0.46	9.719(1)	11.068(5)	905	6.666	92.33		301.6	6.9
$Na_xMo_6Se_{7.5}I_{0.5}$ (R_1'')	0.8	0.85	0.46	9.682(2)	11.740(6)	953	6.823	90.38		317.6	5.2
$Na_xMo_6Se_{7.5}I_{0.5}$ (T_1'')	2.65	2.70	0.46	a = 7.093(3)	b = 7.301(5)	c = 7.075(4)	α = 90.09(5)	β = 96.60(5)	γ = 96.13(5)	360.0	
$Na_xMo_6Se_{7.5}I_{0.5}$ (T_2'')	3.2	3.32	0.46	a = 7.150(3)	b = 7.253(3)	c = 7.132(4)	α = 91.11(4)	β = 96.94(4)	γ = 96.35(4)	364.8	<1
Mo_6Se_7I (R_0''')	—	—	0.98	9.825(0)	10.918(6)	912.8	6.739	93.59		304.2	7.3
$Na_xMo_6Se_7I$ (R_1''')	0.55	0.6	0.98	9.818(1)	11.175(4)	932.9	6.782	92.73		310.9	5.4
$Na_xMo_6Se_7I$ (R_2''')	0.83	0.88	0.98	9.800(1)	11.601(12)	965.1	6.853	91.28		321.7	—
$Na_xMo_6Se_7I$ (T_1''')	2.84	2.90	0.98	a = 7.184(2)	b = 7.263(2)	c = 7.121(2)	α = 92.22(3)	β = 96.38(3)	γ = 95.98(3)	366.8	<1
$Mo_6Se_6I_2$ (R_0'''')	—	—	2.04	9.983(1)	10.807(13)	932.9	6.796	94.51		310.9	4.8
$Na_xMo_6Se_6I_2$ (R_1'''')	0.20	0.30	2.04	9.985(1)	10.894(9)	942.5	6.818	94.27		314.6	4.2
$Na_xMo_6Se_6I_2$(R_2'''')	1.89	1.95	2.04	10.592(2)	11.245(11)	1092.8	7.172	95.11		364.2	<1

Note. a_h, c_h, V_h, and a_r, α_r are lattice parameters for the hexagonal and equivalently rhombohedral unit cells, respectively.

TABLE II

THE OBSERVED *d* SPACINGS AND REFLECTION INTENSITIES OBTAINED BY POWDER X-RAY DIFFRACTION USING COPPER $K\alpha_1$ RADIATION OF $Na_xMo_6S_8$ ($x \simeq 3,4$) ARE COMPARED TO THE VALUES CALCULATED FROM THE LATTICE PARAMETERS OF TABLE I

$Na_3Mo_6S_8$				$Na_4Mo_6S_8$			
hkl	d_{obs} (Å)	d_{calcd} (Å)	I/I_0	*hkl*	d_{obs} (Å)	d_{calcd} (Å)	I/I_0
010	6.935	6.937	80	010	7.051	7.073	80
001	6.625	6.643	100	001	6.789	6.912	100
100		6.601		100		6.874	
$1\bar{1}0$	5.120	5.125	10	$1\bar{1}0$	5.195	5.182	20
$10\bar{1}$	5.020	5.018	7				
$01\bar{1}$	4.859	4.859	8	$01\bar{1}$	4.947	4.950	8
$2\bar{1}0$	3.139	3.142	20	002	3.455	3.456	7
$02\bar{1}$	3.107	3.107	15	$2\bar{1}0$	3.210	3.214	20
$02\bar{1}$	3.035	3.043	4	$02\bar{1}$	3.145	3.145	12
120	2.917	2.918	15	$01\bar{2}$	3.096	3.102	5
$12\bar{1}$	2.749	2.752	15	$1\bar{1}2$	2.955	2.962	15
$2\bar{1}1$	2.725	2.725	14	$21\bar{1}$	2.812	2.816	20
$22\bar{0}$	2.561	2.562	17	112	2.793	2.795	20
$20\bar{2}$	2.506	2.509	8	211	2.671	2.666	7
$02\bar{2}$	2.427	2.429	20	$22\bar{0}$	2.589	2.591	25
$2\bar{2}1$	2.327	2.328	10	022	2.468	2.468	20
$12\bar{2}$	2.279	2.283	20	220	2.353	2.355	22
$03\bar{1}$	2.199	2.201	20	$1\bar{2}2$	2.329	2.332	27
$30\bar{1}$	2.174	2.174	35	$10\bar{3}$	2.239	2.243	15
$13\bar{1}$	2.137	2.140	10	031	2.224	2.229	12
$01\bar{3}$	2.125	2.125	11	212	2.178	2.178	40
122	2.109	2.112	9	$2\bar{2}2$	2.139	2.138	15
221	2.063	2.066	6	$31\bar{1}$	2.074	2.075	30
212	2.038	2.040	8	$11\bar{3}$	2.055	2.058	8
$3\bar{3}1$	1.998	2.001	15	$3\bar{2}0$	2.010	2.012	50
$3\bar{2}0$	1.977	1.977	60	$03\bar{2}$	1.951	1.950	40
$03\bar{2}$	1.920	1.920	18	$12\bar{3}$	1.871	1.870	15
$3\bar{2}1$	1.842	1.844	16	$13\bar{2}$	1.857	1.861	20
$13\bar{2}$	1.826	1.828	14	302	1.835	1.838	10
231	1.688	1.689	18	$14\bar{1}$	1.690	1.691	25
				$41\bar{1}$	1.619	1.620	10

powder patterns are difficult to index, unless additional structural information is available. In this study, a known rhombohedral cell passes through a phase transition to produce a triclinic cell. The indexing of the triclinic cell must bear some rational relationship to that of the rhombohedral cell. A comparison between the R_0 and T_1 phase (see Fig. 3) shows that the rhombohedral $10\bar{1}$ peak clearly splits into the triclinic $10\bar{1}$, $1\bar{1}0$, and $01\bar{1}$ peaks for which an origin can be defined by random assignment. Furthermore the rhombohedral 100 peak splits into two peaks where the higher angle peak integrates to approximately twice the volume of the lower angle peak. This doubling of intensity represents two unresolved lines for which all possible structures are represented by $a > b \simeq c$, $b > a \simeq c$, and $c > a \simeq b$ corresponding to the assignment for the 100, 010, and 001 reflections. A refinement of the three possible models with all observed theta values shows that only one model produces an excellent fit (see Table II). All the triclinic phases were analyzed in the same manner. Although the number of permutations changed from phase to phase each had a single unambiguous solution.

Another prominent feature of Fig. 3 is the similarity of the X-ray patterns d and f which clearly indicates that the $T_1 \leftrightarrow T_2$ transition is perfectly reversible whereas the $R_0 \rightarrow T_1$ transition is irreversible since the X-ray patterns a and g are completely different. The last phase (denoted as R_1) can be completely indexed on the basis of a rhombohedral–hexagonal unit cell. The lattice parameters are reported in Table I and correspond extremely well with the values communicated by Potel (*6*) for $Na_1Mo_6S_8$. After the first cycle the $R_1 \leftrightarrow T_1$ and $T_1 \leftrightarrow T_2$ transitions were found to be perfectly reversible on subsequent cycles.

The room temperature phase diagram for the $Na_xMo_6S_8$ system is reported in Fig. 4 together with electrochemical data. A close relationship of structure to electrochemistry can be observed since peaks in the dV/dx vs x curves occur at values of x for which single phases have been detected. The position of the vertical lines in this diagram was determined by the value of x for which traces of a second phase begin to appear or disappear on the X-ray powder diffraction pattern. Bearing in mind that a second phase can be detected by this technique only if its content is larger than 5%, the range of existence of single-phase products presently reported should not be taken as being precise. In the following several other

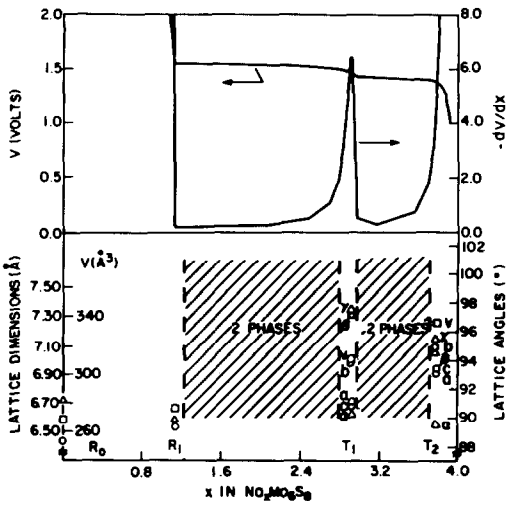

FIG. 4. *In situ* X-ray measurements and electrochemical data for the $Na_xMo_6S_8$ system. (a) Both voltage and dV/dx of a $Na/Na_xMo_6S_8$ cell are plotted as a function of x. (b) Lattice dimensions, (○), lattice angles (△), and unit cell volumes (□) are plotted against x.

phase diagrams will be shown. In order to facilitate their comparison, R_0, R_1, T_1, and T_2 will always represent the unit cell of the initial material, cathode material prior to the second discharge, first triclinic distortion, and second triclinic distortion, respectively. The capital letters R_0, R_1, T_1, and T_2 will be accompanied by one, two, three, and four primes when dealing with the $Na_xMo_6Se_8$, $Na_xMo_6Se_{7.5}I_{0.5}$, $Na_xMo_6Se_7I$, and $Mo_6Se_6I_2$ systems, respectively.

A final point of major concern about these results is the lack of any subtle anomaly in the $V(x)$ curve near $x = 1$ on the first discharge whereas a single phase R_1 forms at $x = 1$ on recharge. This observation may either suggest the coexistence of three phases along the plateau $0 < x < 3$ or more likely indicate that the formation of the R_1 phase can only occur via the T_1 phase. Within the complexity of the X-ray diffraction patterns for these sodium concentrations the first possibility cannot be completely ruled out. However a simple way to test the second eventuality is to cycle a Na/Mo_6S_8 cell to various values of x between 0 and 3. For our suggestion to be correct, one would expect that the insertion of 0.9, 1.6, 2, and 2.8 sodium atoms into Mo_6S_8 will generate 0.3, 0.53, 0.66, and 0.9 mole of $Na_3Mo_6S_8$ (T_1), respectively, which on recharge will give 0.3, 0.53, 0.66, and 0.9 mole of $Na_1Mo_6S_8$ (R_1). Figure 5 shows electrochemical sodium cells based on Mo_6S_8 as cathode material after being discharged down to $x = 0.9$, 1.6, 2, and 2.8 and recharged up to $x = 0.35$, 0.63, 0.75, and 1.10. These values within the accuracy of the electrochemical measurements are in good agreement with our expectations confirming the above suggestion.

$Na_xMo_6Se_8$ System

Figure 6a shows the typical behavior of a Na/Mo_6Se_8 cell over the first two cycles. Like Mo_6S_8, Mo_6Se_8 can insert up to 3.8 sodium atoms per formula unit on discharge to 1 V, with only three of them being removable on recharge resulting in a compound of formula $NaMo_6Se_8$. After the first cycle the voltage composition curves are similar for both Na/Mo_6S_8 and Na/Mo_6Se_8

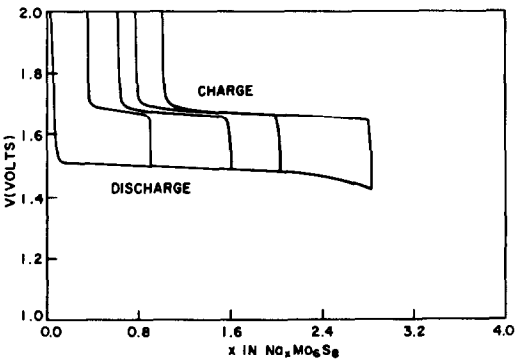

FIG. 5. The first cycle of four $Na/Na_xMo_6S_8$ cells operating at current density of 20 $\mu A/cm^2$ down to $x =$ 0.9, 1.6, 2, and 2.8, respectively, are shown.

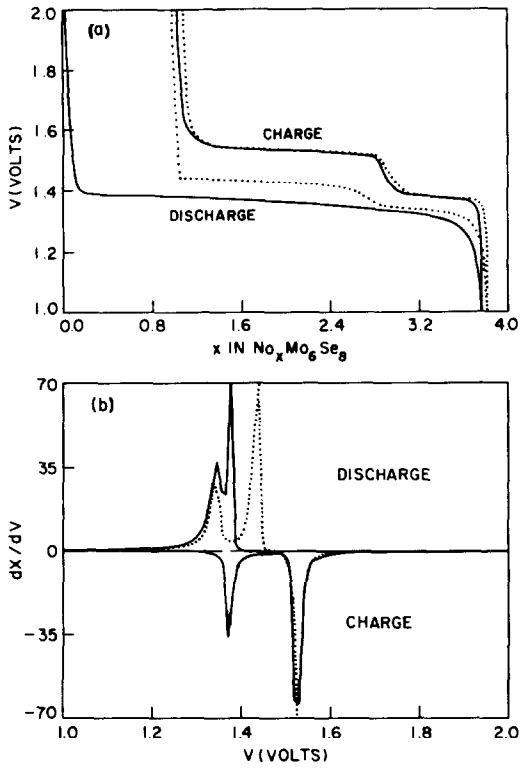

FIG. 6. Constant current (50 μA) cycling data of a $Na/Na_xMo_6Se_8$ cell. Both $V(x)$ curves and dx/dV vs V plots are shown in (a) and (b), respectively. Solid and dotted line refer to first and second cycle, respectively.

cells with the presence of two plateaus on both charge and discharge. However, the potential at the discharge plateaus is lower for the selenides than for the sulfides 1.44 and 1.34 V instead of 1.54 and 1.44 V, respectively, indicating a lower free energy of the reaction of the selenide compared to the sulfide compounds. Previous studies (*10*) of the $Li_xMo_6X_8$ systems have led to similar observations.

An interesting feature of Fig. 6 is the apparent difference between the shape of the charge and discharge curves during the first cycle. The first discharge curve suggests the presence of two single phases of nominal composition $x = 0$ and $x = 4$ connected by a plateau whereas the charge curve seems to indicate the presence of three single phases at $x = 3.8$, 3, and 1, respectively, interconnected by two plateaus. The absence of a detectable voltage anomaly on the first discharge at $x = 3$ may simply indicate the absence of a single phase at such composition or more likely that the free energy of formation of this phase is so close to that of the $x = 4$ phase that it cannot be detected on the $V(x)$ curves. The differential capacity plot (Fig. 6b) unambiguously confirms the latter possibility, since two well-defined peaks separated by only 0.02 V appear on discharge. These two peaks arise from the presence of two plateaus in the discharge curve interconnecting three single-phase domains. This finding suggests a similar sodium intercalation process for both binary phases Mo_6S_8 and Mo_6Se_8. A final point to note is the jump in potential of about 0.05 V between the first and second discharge curve. This may simply result from a structural difference between the initial and final cathode material Mo_6Se_8 and "$NaMo_6Se_8$," respectively, so that the chemical potential of sodium in both materials is different.

To substantiate these suggestions *in situ* X-Ray diffraction measurements were performed on a Na/Mo_6Se_8 electrochemical cell. The results of this study are shown in Fig. 7. We found that as sodium intercalation proceeds the binary phase Mo_6Se_8 (R_0') transforms discontinuously into a single phase of nominal composition $x = 3.8$. This phase has been completely indexed on a basis of a triclinic unit cell (denoted as T_2') for which lattice parameters are reported in Table I. It is important to mention that X-ray powder patterns taken at intermediate values of x reveal two sets of Bragg peaks corresponding to the R_0' phase and another phase "T_1'" (different than T_2') at low values of x, and to the "T_1'" and T_2' phases at high

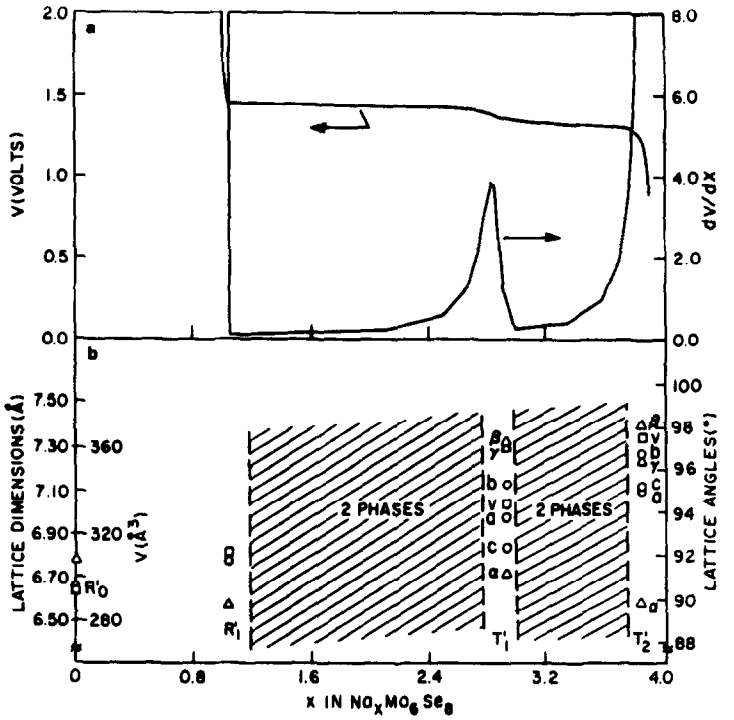

FIG. 7. Room temperature phase diagram (b) of the $Na_xMo_6Se_8$ system established by means of *in situ* X-ray diffraction measurements is shown along with the voltage composition curve (a). ○, △, and □ refer to lattice dimension, lattice angles, and unit cell volumes, respectively.

sodium content. Attempts to completely isolate this phase during the first discharge were unsuccessful even by using low current drains. Each time either the R'_0 or T'_2 phases were present.

On recharge one finds that the T'_2 phase transforms discontinuously into a single phase of composition $Na_3Mo_6Se_8$ which crystallizes in a triclinic unit cell (denoted as T'_1) whose lattice parameters are reported in Table I. Further removal of sodium atoms results in a third new hexagonal–rhombohedral phase (denoted as R'_1) of formula $Na_1Mo_6Se_8$ with the following lattice parameters $a_r = 6.780(1)$ Å, $\alpha_r = 89.86$ Å. X-Ray diffraction patterns have shown that the R'_1–T'_1 and T'_1–T'_2 are reversible and furthermore of first order as expected from the asymmetric peaks at 1.34 and 1.44 V in the dx/dV vs V plot on discharge.

$Mo_6X_{8-y}I_y$ Phases

The typical behavior over several cycles of electrochemical cells based on binary halochalcogenides $Mo_6Se_{8-y}I_y$ ($y = 0.5$, 1, and 2) as cathode materials are reported in Fig. 8. Interesting features can be observed, namely that the maximum uptake of guest ions (number of sodium atoms to enter the structure on discharge) is strongly correlated to the iodide content (y) of the cathode material. For instance, x_{max} decreases from 3.4 to 2 as y increases from 0.5 to 2. This result, as we will see shortly, is consistent with both ionic and band structure considerations.

None of the above $Na/Na_xMo_6Se_{8-y}I_y$ cells can be completely recharged up to potentials of about 2.7 V; therefore their reversibility increases with increasing iodide

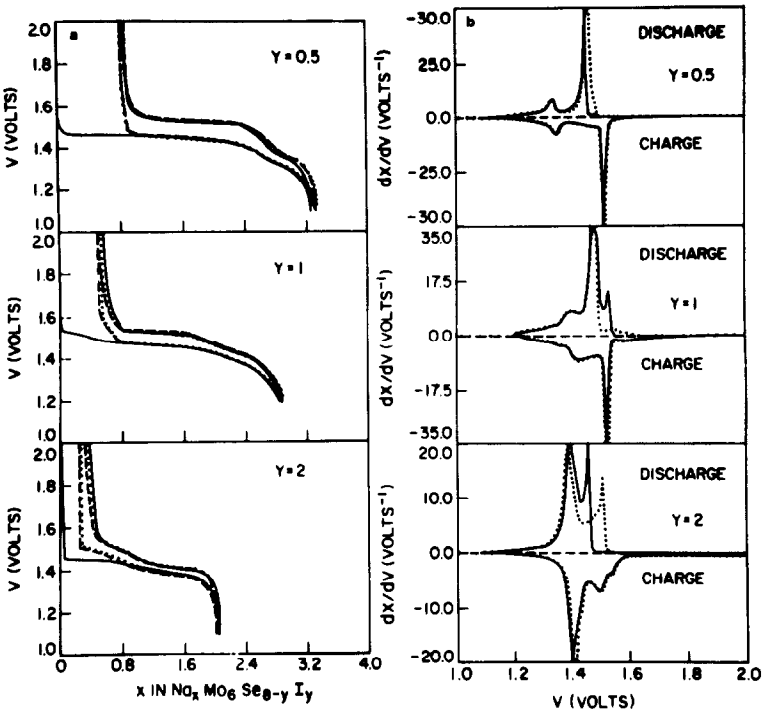

FIG. 8. Cycling data made at 150 $\mu A/cm^2$ for several $Na/Na_xMo_6Se_{8-y}I_y$ cells (y = 0.5, 1, 2). Both $V(x)$ curves (a) and dx/dV vs V curves (b) are shown. Solid, dotted, and dashed line refer to first, second, and third cycle.

content. Indeed the voltage-composition curves show that the amount of sodium (x_{min}) left in the cathode material after a complete cycle decreases from 0.8 to 0.2 as y increases from 0.5 to 2 (Fig. 8a). The values of x for the recharged materials, determined by atomic absorption analysis, confirm the above trend and agree quite well with the electrochemical ones (Table I).

A common feature in the $V(x)$ curves (Fig. 8) is the presence of several voltage drops most likely related to sodium-induced structural instabilities. The values of x (sodium content) at which these anomalies occur are strongly dependent upon the iodide content (y) in the cathode material $Na_xMo_6Se_{8-y}I_y$. The domains of zero slope voltage which connect these anomalies appear as peaks in the dx/dV vs V plot (Fig. 8b). As mentioned earlier, the asymmetric peaks observed during the second discharge at v = 1.45 and 1.33 V for $Na/Mo_6Se_{7.5}I_{0.5}$, at v = 1.59 and 1.49 V for Na/Mo_6Se_7I, and at v = 1.50 V for $Na/Mo_6Se_6I_2$ lead to the expectation of first order transitions. Conversely, the symmetric peaks at v = 1.43 and 1.39 V for the Na/Mo_6Se_7I and $Na/Mo_6Se_6I_2$ cells, respectively, suggest either second order phase transitions or are reminiscent of the behavior of single phases. *In situ* X-ray diffraction measurements have been undertaken to test these predictions. The room temperature phase diagram and the second electrochemical discharge curve are shown all together in Figs. 9a, 9b, and 9c for the $Na_xMo_6Se_{8-y}I_y$ systems with x = 0.5, 1, and 2, respectively.

At y = 0.5 the phase diagram is similar to that of $Na_xMo_6Se_8$ with a rhombohedral

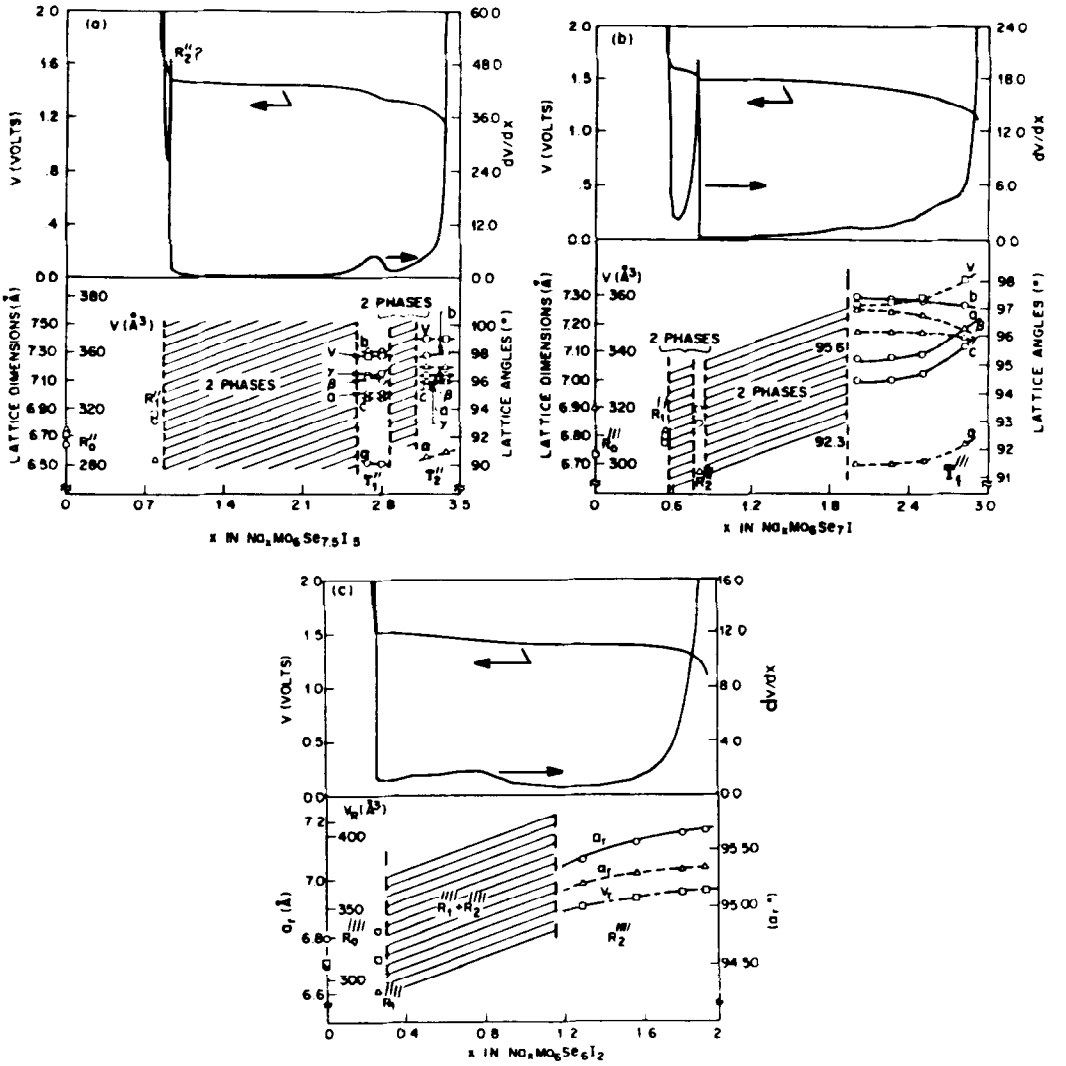

FIG. 9. Room temperature phase diagrams for the $Na_xMo_6Se_{8-y}I_y$ systems established by means of *in situ* X-ray diffraction measurements performed on $Na/Na_xMo_6Se_{8-y}I_y$ cells run at 15 $\mu A/cm^2$ are shown. a, b, and c refer to the $Na_xMo_6Se_{1.7}I_{1.5}$, $Na_xMo_6Se_7I$, and $Na_xMoSe_6I_2$ systems, respectively. ○, △, and □ refer to lattice dimensions, lattice angles, and unit cell volumes, respectively.

phase R″ which discontinuously transforms into a first triclinic phase T_1'' ($x \simeq 2.8$) and then discontinuously into a second triclinic phase T_2'' ($x \simeq 3.3$). The two transitions are reversible. Increasing iodine substitution results in drastic modifications of the phase diagram, indeed at $y = 1$, we observe that the rhombohedral phase R_1''' ($x \geq 0.55$) transforms discontinuously into a second new rhombohedral phase (denoted as R_2''') with a narrow range of existence. One should mention that a R_2'' phase most likely exists for the $Mo_6Se_{7.5}I_{0.5}$ system as indicated by the peak in the dV/dx vs x plot around $x = 0.9$. However, we were not able to isolate such a phase by *in situ* X-ray mea-

surements. Further sodium intercalation induces a first order phase transition into a triclinic phase T_1''' which exists over a wide range of composition, $2.0 < x < 3.0$. Although the derivation of the lattice constants was performed in a relatively mechanical manner, the consistency of the results (Table I) is quite remarkable. Every triclinic cell has the relationship $b > a \simeq c$, $\alpha < \beta \simeq \gamma$, suggesting that each $R \leftrightarrow T$ transition occurs through the same structural mechanism.

Finally for the $Na_xMo_6Se_6I_2$ system, as the sodium intercalation proceeds, the R_1''' phase transforms discontinuously into a phase R_2''' which exists over a wide range of composition $1.3 < x < 2$. The general trend arising from the X-ray results is that with increasing iodide content the $T_1 \leftrightarrow T_2$ and $R_1 \leftrightarrow T_1$ phase transitions vanish and a new $R_1 \leftrightarrow R_2$ phase shows up. In other words, iodine substitution stabilizes the host structure against distortions to triclinic phases. We recently observed a similar trend with lithium instead of sodium. The origin of such behavior has been intensively discussed and we will refer the reader to this work (*24*). A remarkable point to note in Fig. 9 is the perfect correlation between X-ray and electrochemical data. Indeed, each single-phase product corresponds to a maximum in the dV/dx vs x plot while a multiphase domain appears as minimum. Conversely, the multiphase domains appears as peaks in the dx/dV vs V plot (Fig. 8). The nature of the phase transitions previously deduced from the shape of these peaks is in good agreement with the X-ray data. From an academic point of view the family of compounds $Mo_6X_{8-y}I_y$ constitutes an ideal example to illustrate the perfect relationship of structure to electrochemistry.

Among the chalcogenide compounds, a higher free energy of reaction has always been observed for the sulfides than for the selenides. On this basis one would expect the electrochemical formation of "$Na_2Mo_6S_6I_2$" to be easier than that of $Na_2Mo_6Se_6I_2$. Surprisingly, cycling data collected on several $Na/Na_xMo_6S_6I_2$ test cells have revealed the inability to intercalate sodium into $Mo_6S_6I_2$. This unexpected result is difficult to explain rationally.

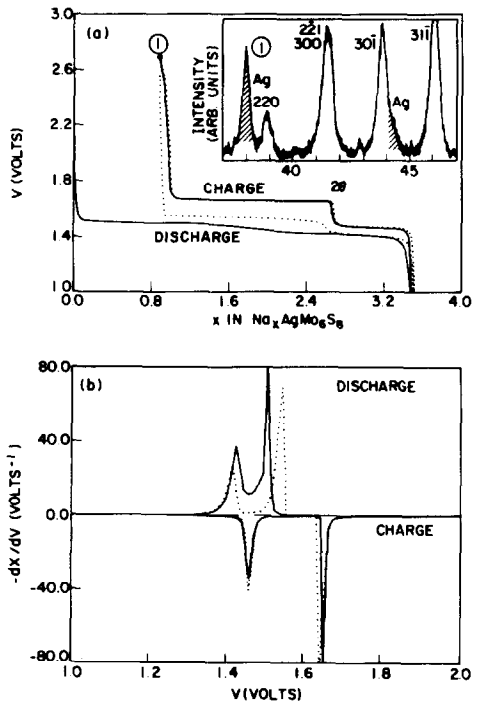

FIG. 10. Typical behavior of a $Na/Na_xAgMo_6S_8$ made at 150 $\mu A/cm^2$ over the two first cycles. Both $V(x)$ curves (a) and dx/dV vs V plots (b) are shown. Solid and dotted line refer to the first and second cycle, respectively. Insert shows the X-ray diffraction pattern of the cathode material collected at position labeled 1 on the $V(x)$ curve. Peaks due to free silver metal are crosshatched.

$Na_xAgMo_6S_8$ System

The electrochemical behavior of a sodium cell based on the ternary Chevrel phase $AgMo_6S_8$ as cathode material is shown in Fig. 10. A striking feature arises from the shape of the $V(x)$ curves which is similar, after the first discharge, to that exhibited by a Na/Mo_6S_8 cell. The dx/dV vs V

measurements can be used as an "electrochemical potential spectrum" for any material. Figure 10b shows the spectrum characteristic of $Na_xMo_8S_8$ after the first cycle. Both findings suggest that after the first discharge the silver atoms are no longer incorporated into the lattice but are most likely dispersed as elemental metal in the cathode material, so that the host material behaves as the binary phase Mo_6S_8 with respect to sodium intercalation.

The above suggestion is confirmed by the insert of Fig. 10a which represents the X-ray diffraction pattern of the cathode material after a complete cycle. In addition to the Bragg peaks corresponding to the pure $Na_1Mo_6S_8$ phase one notes two extra peaks due to silver metal. This is clear evidence that the ternary Chevrel phase $AgMo_6S_8$ reacts with sodium by the displacement reaction

$$AgMo_6S_8 + Na \rightarrow Na_xMo_6S_8 + Ag$$

which is complete after the first cycle. The removal of silver by sodium implies that sodium modifies the chemical potential of Ag in the host structure in a way that it becomes equal to that of Ag in silver metal. The above reaction is not specific to Chevrel phases with Ag but also occurs with other ternary metal atoms such as indium or copper. In a recent study (*10*) we even reported similar reactions to occur with lithium of sodium. In this latter case the reaction was slower since several electrochemical cycles were required to completely remove the ternary metal atom. The rate of the displacement reaction appears to be strongly dependent on the nature of the ternary element. There are two possible explanations for such observations. First it is known that in the Chevrel phase structure the lithium atoms generally sit on tetrahedral sites around the $\bar{3}$ axis while sodium atoms prefer to be on the $\bar{3}$ axis site as is the case for silver. As lithium intercalation into $AgMo_6S_8$ proceeds, the Li^+ ions, due to their small size (0.53 Å), can first occupy the tetrahedral sites available in the $AgMo_6S_8$ host matrix before competing for the silver site (displacing Ag ions). The available sites in $AgMo_6S_8$ are certainly not large enough to accommodate large ions such as Na^+ (0.95 Å); furthermore, the migration of Na^+ into these sites will be blocked by Ag^+ ions (1.26 Å) sitting on the $\bar{3}$ axis. Then in order to enter the matrix, the sodium ions have to first liberate the inner sites occupied by silver, and as a result, the displacement of silver should occur during the first discharge as observed experimentally. Another possibility arises from the fact that the intercalation of four sodium atoms into Mo_6S_8 results in an increase of the unit cell volume (265 to 338 $Å^3$) twice as large as the increase caused by the insertion of four lithium atoms (263 to 292 $Å^3$). One might then expect the "$AgMo_6S_8$" matrix to expand more when sodium atoms intercalate. As a result, the diffusion of the silver atoms would be enhanced. This explanation is at least consistent with the experimental observation.

Ambient Stability of the Sodium Chevrel Phases

Electrochemical data (i.e., the recharge curves) have shown that the oxidation of the sodium Chevrel phases $Na_xMo_6X_{8-y}I_y$ (i.e., removal of sodium) occurs below 1.7 V. However, we found that this oxidation is incomplete since sodium cannot be removed from the $Na_1Mo_6X_8$, $Na_{0.8}Mo_6Se_{7.5}I_{0.5}$, $Na_{0.5}Mo_6Se_7I$, and $Na_{0.2}Mo_6Se_6I_2$ phases (denoted earlier as R_1), even with potentials as high as 3 V. It is now important to recall that the reaction of sodium with water occurs at 1.9 V. Consequently, on the basis of these values one should expect the sodium phases (denoted earlier as R_2, T_1, T_2) with an oxidation potential lower than 1.9 V to react with moisture while the

R_1 phases alluded to above should be air stable.

This is directly confirmed by X-ray diffraction measurements since the compounds $Na_3Mo_6S_8$ and $Na_{3.9}Mo_6S_8$, for instance, after being exposed a short time to air, have the same lattice parameters as $Na_1Mo_6S_8$. The mobility of sodium into the $Na_xMo_6S_8$ phases is certainly high and as a result, the sodium comes out of the channels by reacting with water to form NaOH, hydrogen, and the air stable phase $Na_1Mo_6S_8$. No sodium atoms can be removed from this latter phase even after washing it for several days in water. The $Na_xMo_6Se_{8-y}I_y$ systems behave similarly with respect to water. The T_1, T_2, or R_2 phases were always found to convert immediately to the R_1 phases after short exposure to air. These observations are quite consistent with the electrochemical results and furthermore indicate that caution should be exercised in handling these materials. This high reactivity may explain the failure encountered in isolating the $Na_xMo_6X_8$ phases $x \simeq 3$ and 3.9 up to now.

Physical Properties

The $Na_xMo_6X_{8-y}I_y$ single-phase products were studied for their superconducting and magnetic properties. The superconducting critical temperatures (T_c) are reported in Table I along with the structural parameters. Among the Chevrel phase compounds containing the same ternary element, a difference in T_c of about ± 3 K is usually observed between the sulfide and selenide phases (*1*). However, the sodium Chevrel phases do not obey this empirical relation since $NaMo_6S_8$ and $NaMo_6Se_8$ superconduct at 9.1 and 8.9 K, respectively. Neither of the sodium phases with a triclinic unit cell superconduct down to 1 K. This is not surprising since in many other compounds, such as $EuMo_6S_8$, $BaMo_6S_8$, or $SrMo_6S_8$ (*25*), the presence of triclinic distortions has been used to explain the absence of superconductivity. According to previous work (*26, 27*) the increase in unit cell volume observed for the halochalcogenide compounds $Na_xMo_6Se_{8-y}I_y$ as sodium enters the structure would lead to the expectation of high T_c. The opposite trend is clearly seen in Table I.

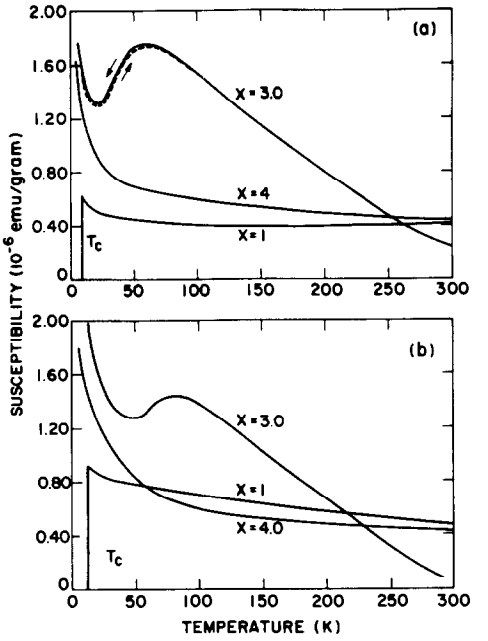

FIG. 11. Temperature-dependent susceptibility of several members of the series $Na_xMo_6X_8$, (a) X = S, x = 1, 3, 4; (b) X = Se, x = 1, 3, 4. The arrows distinguish between cooling or warming of the sample.

The magnetic measurements were performed on several materials from 4.2 to 300 K. Figures 11a and b show the measured susceptibility for the $Na_xMo_6S_8$ and $Na_xMo_6Se_8$ single-phase products. A mild temperature dependence of the susceptibility is observed for the compounds with $x = 1$ in contrast to a more pronounced temperature dependence for the phases with $x = 4$. This behavior may be explained as follows. The sodium atoms enter the structure as donating electrons to the Mo_6X_8 clusters. With four sodium atom, the number of electrons per Mo_6X_8 unit reaches the upper limit (*24*) at which the compounds become semicon-

ducting (*27*). In that range of sodium concentration ($x_{max} \simeq 4 - \varepsilon$) we are dealing with a nearly full conduction band and it may be that few electrons become localized so that they contribute to the susceptibility. This will be at least consistent with the magnetic data as well as with the absence of T_c for the $Na_xMo_6X_8$ phases ($x \simeq 4$). The most striking feature of Fig. 11 arises from the susceptibility dependence of the $Na_3Mo_6X_8$ phases which present a large anomaly as the temperature is lowered. This anomaly does not give rise to hysteresis and furthermore shifts to higher temperature in going from the sulfide to the homolog selenide phase. An interesting comparison can be made with the $Li_{3.2}Mo_6X_8$ phases where a similar analogy with an onset temperature higher for the selenide than for sulfide has been reported (*10*). This anomaly may be ascribed either to a temperature-induced phase separation (the $Na_3Mo_6S_8$ phase decomposes onto $Na_{3-x}Mo_6S_8$ and $Na_{3+x}Mo_6S_8$ phases as in the $Cu_xMo_6S_8$ system) or to temperature-induced lattice instabilities (*25*) (distortion of the triclinic unit cell). At the present time, without low-temperature X-ray measurements, it is impossible to distinguish between the two possibilities.

Discussion

The Chevrel phases made up of Mo_6X_8 units with large empty channels running along the hexagonal axis are ideal candidates for use in the study of intercalation reactions. The physics and chemistry of the intercalation process into these open-structure phases depend mainly upon the size and symmetry of the cavity, the electronic structure of the host material as well as upon the size, formal valence, and reduction potential of the guest species. Within the same host structure one would expect the sodium intercalation process to be in a certain sense similar to that of lithium previously reported (*10–12*), since lithium and sodium differ only in their size. The present work has revealed several striking differences, the most surprising one being the irreversibility of the sodium intercalation process into these phases. The following paragraphs will address the origin of these differences.

Sodium intercalation into the binary phase Mo_6X_8 results in a discontinuous distortion of the rhombohedral cell R_0 into a triclinic phase T_1 at ($x \simeq 3$). Such a transition is accompanied by volume increases (265 to 338 Å^3) and (292 to 367 Å^3) for the sulfide and selenide system, respectively. The R_0 phase (Mo_6X_8) with $\alpha_r \simeq 91.5°$ presents two types of sites available for intercalation, a large eightfold cavity (site 1) compressed along the $\bar{3}$ axis with a maximum occupancy of 1, and six small tetrahedral sites (site 2) forming a ring around the $\bar{3}$ axis. As α_r increases, the type 1 sites (donut shaped) transform discontinuously into a ring of six other tetrahedral sites (called inner sites) in contrast to the type 2 sites (called outer sites). Such transformations result in a range of instability in α_r. The occupancy of these sites by sodium will be determined by the site energy (e.g., energy required to place sodium atoms into site 1 or site 2) which changes as intercalation proceeds. In order to introduce three or four sodium atoms into the structure it appears that sodium would have to occupy tetrahedral sites. This implies that as the sodium intercalation proceeds, α_r, as well as the unit cell volume would have to increase to make more sites available for sodium as observed experimentally. The $T_1 \leftrightarrow T_2$ transition can be ascribed either to an order–disorder reaction of the sodium atoms into the type 1 and 2 sites alluded to above as in the $Cu_xMo_6S_8$ system or to electronic driven lattice instabilities as observed with the divalent Chevrel phases (Eu, Ba, . . .). Without neutron data to determine atomic positions and bond lengths we cannot distinguish between these two possibilities.

On recharge the triclinic phase T_1 does not convert to Mo_6X_8 but to the more thermodynamic stable phase $Na_1Mo_6X_8$. These compounds with a rhombohedral angle of 89.7° belong to type I Chevrel phases (e.g., the Na atom is well localized on the $\bar{3}$ axis). The driving force for the occupancy of the $\bar{3}$ axis site, instead of the tetraheral sites, most likely results from a large difference in energy between these two sites. The mobility of the ternary element into type 1 materials is known to be small, and as a result, removal of sodium atoms should be difficult, in agreement with our observations.

We now discuss the halochalcogenide compounds which also show an irreversible intercalation process resulting in compounds of formula $Na_xMo_6Se_{8-y}I_y$ with rhombohedral angles greater than 90°. This observation may indicate that these phases are type II compounds (ternary atoms out of $\bar{3}$ axis). However, the gap in α_r between type I and type II phases can occur at values larger than 90° (for example, 92–94° in the $Li_xMo_6X_8$ system). Based on this, it is quite reasonable to assume that sodium atoms sit on the $\bar{3}$ axis in the ternary halochalcogenide phases (R_1) despite α_r being greater than 90°. Then, like $Na_1Mo_6X_8$, one would expect the R_1 phases to be air stable as we have observed experimentally. Another remarkable finding among the R_1 phases arises from their sodium content (x) which decreases with increasing iodide substitution. This result may be explained in terms of site energy as follows. Sergent *et al.* (*29, 30*) have shown that the substitution of chalcogen by iodine into the binary phases Mo_6X_8 can take place only with the two chalcogen positions on the $\bar{3}$ axis resulting in compounds of formula $Mo_6X_{8-y}I_y$ with $y \leq 2$. A complete solid solution $0 \leq y \leq 2$ exists for the $Mo_6Se_{8-y}I_y$ system, whereas the two end members $y = 0$ and $y = 2$, exist only for the homologous sulfide system. As iodine is introduced into the host lattice, the sodium site X–Na–X transforms into three different sites X–Na–X, X–Na–I, and I–Na–I with a population of $(1 - y/2)^2$, $y(1 - y/2)$, and $(y/2)^2$, respectively. If these $\bar{3}$ axis sites were equally occupied one would expect the sodium content (x) intercalated into the R_1 phases to be independent of iodine substitution (y) and equal to 1. The present results clearly rule out this possibility suggesting then that these sites are of different energy. The larger ionic radius of I^{-1} over Se^{-2} (2.16 instead of 1.98 Å), as well as the smaller coulombic interactions between I^{-1}–Na^+ compared to X^{-2}–Na^+, led us to predict that the I–Na–I site is energetically unfavorable. Both our data, which show that x_{min} is close to zero (0.2) in $Na_xMo_6Se_6I_2$ or equal to zero in $Na_xMo_6S_6I_2$, and our inability to synthesize $M_xMo_6X_6I_2$ phases with large ternary metal atoms (Pb,Sn) strongly support the above prediction. The statistical model that we recently constructed for the $Li_xMo_6X_{8-y}I_y$ system (see Fig. 8, Ref. (*24*)) may be used to determine which one of the resulting X–Na–I or X–Na–X sites is more energetically favorable for sodium. On this plot the experimental points ($x_{min} = 0.85$, $y = 05$; $x_{min} = 0.60$, $y = 1$) are situated just below the curve of equation $P = 1 - y^2/4$ which represents the total occupancy of both X–Na–X and X–Na–I sites. This indicates that the number of X–Na–X and X–Na–I available sites at a given value of y determines the maximum uptake of sodium atoms on the $\bar{3}$ axis for the R_1 phases whereas previous work (*24*) has shown that the maximum value of x in the homolog $Li_xMo_6Se_{8-y}I_y$ phases (R_1) is determined only by the occupancy of the X–Li–X sites. Such differences may tell us only that the energy of the ternary metal atoms on the $\bar{3}$ axis site is not only dependent upon the closest chalcogen atoms but also may be affected by more distant atoms as the size of the guest ion increases.

An important question still remaining about these molybdenum chalcogenide compounds is whether the maximum uptake of guest ions into Mo_6X_8 is determined

by electronic rather than structural factors. In an attempt to answer this point we will now comment on our electrochemical results with respect to both electronic structure of the "host" and bonding models. Anderson (*31*), Hughbanks (*32*), and Bullet (*33*) have performed band structure calculations for several of these phases (Mo_6Se_8, $PbMo_6Se_8$). All the treatments agree with the presence of a narrow E band (made out of Mo d states) at the Fermi level situated just below an energy gap estimated at 24 electrons per Mo_6 cluster. This upper limit number was early proposed by Yvon (*34*) as the result of the observation that the Mo_6 cluster needs $24e^-$ to form 12 maximum covalent bonds. Another finding of these calculations was that the chalcogen p band situated below the E_g band is completely filled, so that a complete charge transfer from the guest ternary atom to the Mo_6 cluster should take place, as observed experimentally by Yvon (*34*). Then according to the above remarks $[Mo_6^{+}S_8^{-2}]^{+4}$ with 20 electrons and $[Mo_6^{+2}X_{8-y}^{-2}I_y^{-1}]^{+(4-y)}$ with $(20 + y)$ electrons per Mo_6 unit should be capable of adding 4 or $4 - y$ electrons (i.e., ternary metal atoms (M^+)), respectively, before becoming semiconducting, assuming that the sodium-induced triclinic distortions do not close the energy gap. This point is clearly confirmed in Fig. 12b which shows the first electrochemical discharge curves of several $M/Mo_6X_{8-y}I_y$ test cells (M = Na). Indeed one notes that Mo_6X_6 can accommodate four sodium atoms while $Mo_6Se_{7.5}I_{0.5}$, Mo_6Se_7I, $Mo_6Se_6I_2$, with initially 20.5, 21, and 22 electrons per Mo_6 cluster, can accommodate only 3.5, 3, and 2 alkali atoms, respectively, before observing a sharp drop in potential. In the absence of evidence for phase transitions at these sodium concentrations the observed voltage drop is directly related to the complete filling of the E_g band alluded to above as follows. The voltage of an intercalation cell is determined by the energy of the charge transferred electrons. As the sodium insertion proceeds, an equal number of electrons occupies the empty states of the partially unfilled valence band (E_g) in the host material. When this band is filled (24 electrons) the transferred electrons have to occupy an electronic state in the next band. If the compound is semiconducting, the next band (e.g., the next empty electronic state) is much higher in energy resulting in a sharp drop in voltage. The sodium concentrations at which the voltage anomalies occur (Fig. 12a) agree amazingly well with the values predicted from band structure calculations. Another striking feature of Fig. 12 is that the maximum ternary element content in these materials, within the accuracy of the electrochemical measurements, is independent of the guest species sodium or lithium even though Na^+ is nearly twice as large as

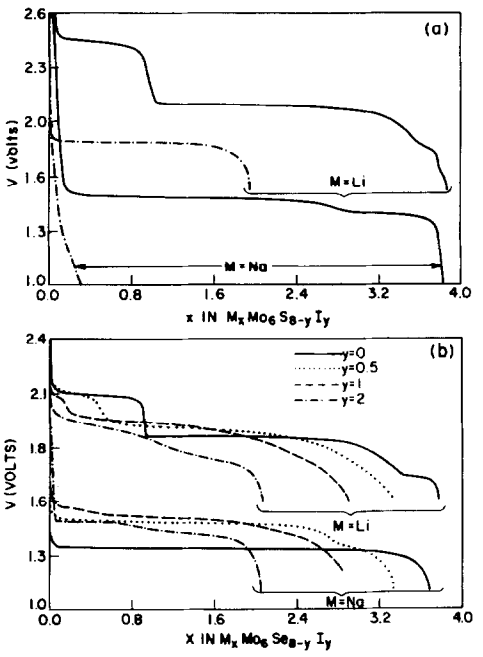

FIG. 12., The first electrochemical discharge curves of several $M/M_xMo_6X_{8-y}I_y$ cells (M = Na, Li) operated at a current density of 150 $\mu A/cm^2$ are shown for X = sulfur (a) and X = selenium (b) separately.

Li^+ (0.97 versus 0.53 Å). This observation led us to conclude that the maximum uptake of alkali atoms Li and Na into Mo_6X_8 structures is determined merely by the electronic structure of the host. However, the inability to intercalate sodium into $Mo_6S_6I_2$ suggests that structural factors have also to be taken into account. These structural factors become predominant for the type I Chevrel phase $M_xMo_6X_8$ phases which can exist only with $x = 1$, even though the E_g band is incompletely filled.

Conclusion

We have reported the electrochemical insertion of sodium into the binary $Mo_6X_{8-y}I_y$ phases and some properties of these new phases. We found an irreversible intercalation process resulting in stable compounds of formula $Na_xMo_6X_{8-y}I_y$. The sodium content (x_{min}) decreases with increasing y. This behavior was explained in terms of available vacant sites and site energy. We showed, at least for small atoms (Li, Na), that the maximum uptake of guest ions into the host materials, $Mo_6X_{8-y}I_y$, is determined mainly by electronic rather than structural factors. *In situ* X-ray diffraction measurements revealed sodium-induced lattice instabilities. Three single phases $R_1(x \simeq 1)$, $T_1(x \simeq 3)$, and $T_2(x \simeq 4)$ with rhombohedral, triclinic unit cells (T_1 and T_2), respectively, were discovered. The nature and existence regions of these phases are affected by iodine substitution (y). The $R_1 \leftrightarrow T_1$ and $T_1 \leftrightarrow T_2$ transitions vanish and a new $R_1 \leftrightarrow R_2$ transition occurs with increasing y. Structural changes correlate perfectly with electrochemical data. The phase transitions appear as peaks in the dx/dV vs V plot, whereas single-phase compounds or solid solutions give rise to voltage anomalies in the $V(x)$ curves and to peaks in the dV/dx vs x plot. Finally, physical properties measurements have revealed anomalies in the temperature-dependent susceptibility curves for the $Na_xMo_6X_8$ phases most likely connected to structural instabilities which in turn may be linked to the particular type of site occupied by the Na^+ cations in the channels of Mo_6X_8 Chevrel phases. However, more knowledge of both the position of the sodium atoms and bond lengths in the $Na_xMo_6X_{8-y}I_y$ phases will be of great importance for a complete understanding of both the sodium- and temperature-induced lattice instabilities reported herein. Further structural work such as neutron experiments, which are now in progress, should help us to determine the origin of these structural instabilities.

Acknowledgments

We thank J. H. Wernick and D. W. Murphy for their enlightening discussions concerning the paper.

References

1. K. Yvon, *Curr. Top. Mater. Sci.* **3,** 53 (1979).
2. Ø. Fisher, *Appl. Phys.* **16,** 1 (1978).
3. M. B. Maple and Ø. Fisher, "Superconductivity in Ternary Compounds I, II," Springer-Verlag, Berlin (1982).
4. M. Marezio, P. D. Dernier, J. P. Remeika, E. Corenzwit, and B. T. Matthias, *Mater. Res. Bull.* **8,** 657 (1973).
5. R. Chevrel and M. Sergent, *in* "Superconductivity in Ternary Compounds I," (Ø. Fisher and M. B. Maple, Eds.), Springer-Verlag (1982).
6. M. Potel, communicated to authors of Ref. (*5*).
7. G. J. Dudley, K. Y. Cheung, and B. C. H. Steele, *J. Solid State Chem.* **32,** 259 (1980).
8. K. Y. Cheung and B. C. H. Steele, *Solid State Ionics* **1,** 337 (1980).
9. M. Tovar, L. E. Delong, D. C. Johnston, and M. B. Maple, *Solid State Commun.* **30,** 551 (1979).
10. J. M. Tarascon, F. J. DiSalvo, D. W. Murphy, G. W. Hull, E A. Rietman, and J. V. Waszczak, *J. Solid State Chem.* **54,** 204 (1984).
11. P. J. Mulhern and R. R. Haering, *Canad. J. Phys.* **62,** 527 (1984).
12. S. T. Coleman, W. R. McKinnon, and J. R. Dahn, *Phys. Rev. B: Condens. Matter.* **29,** 4147 (1984).

13. J. R. DAHN AND W. R. MCKINNON, *Phys. Rev. B,* 31, 484 (1985).
14. J. R. DAHN AND W. R. MCKINNON, *Phys. Rev. B,* 31, 3084 (1985).
15. R. CHEVREL, M. SERGENT, AND J. PRIGENT, *J. Solid State Chem.* **3,** 515 (1971).
16. N. E. ALEKSEEVSKII, N. M. DOBROVOL'SKII, AND V. I. TSEBRO, *JETP Lett.* **23,** 639 (1976).
17. R. SCHÖLLHORN, M. KUMPERS, AND J. O. BESENHARD, *Mater. Res. Bull.* **12,** 781 (1977).
18. R. SCHÖLLHORN, M. KUMPERS, AND D. PLORIN, *J. Less-Common Met.* **58,** 55 (1978).
19. J. M. TARASCON, J. V. WASZCZAK, G. W. HULL, F. J. DISALVO, AND L. BLITZER, *Solid State Commun.* **47,** 973 (1983).
20. J. M. TARASCON AND D. W. MURPHY, *Phys. Rev. B: Condens. Matter.* (1986).
21. W. R. MCKINNON AND R. R. HAERING, *Mod. Aspects Electrochem.* **15,** 235 (1983).
22. A. H. THOMPSON, *J. Electrochem. Soc.* **126,** 608 (1979).
23. J. R. DAHN AND W. R. MCKINNON, *J. Electrochem. Soc.* **131,** 1823 (1984).
24. L. TER HARR, F. J. DISALVO, AND J. M. TARASCON, to be published.
25. R. BAILLIF, A. DUNAND, J. MULLER, AND K. YVON, *Phys. Rev. Lett.* **47,** 672 (1981).
26. O. BARS, J. GUILLEVIC, AND D. GRANDJEAN, *J. Solid State Chem.* **6,** 48, 335 (1973).
27. D. C. JOHNSTON AND R. N. SHELTON, *J. Low Temp. Phys.* **26,** 561 (1977).
28. R. FLUKIGER, R. BAILLIF, J. MULLER, AND K. YVON, *J. Less-Common Met.* **72,** 193 (1980).
29. A. PERRIN, R. CHEVREL, M. SERGENT, AND Ø. FISHER, *J. Solid State Chem.* **33,** 43 (1980).
30. M. SERGENT, Ø. FISHER, M. DECROUX, C. PERRIN, AND R. CHEVREL, *J. Solid State Chem.* **22,** 87 (1977).
31. O. K. ANDERSEN, W. KLOSE, AND H. NOHL, *Phys. Rev. B: Condens. Matter.* **17,** 1209 (1978).
32. T. HUGHBANKS AND R. HOFFMAN, *J. Amer. Chem. Soc.* **105,** 1150 (1983).
33. D. W. BULLET, *Phys. Rev. Lett.* **39,** 664 (1977).
34. K. YVON AND A. PAOLI, *Solid State Chem.* **24,** 41 (1977).